
SELF-SUPERVISED PSEUDO-COLORIZING OF MASKED CELLS

A PREPRINT

Royden Wagner*

Perception Group, Institute of Measurement and Control Systems
Karlsruhe Institute of Technology (KIT)

Carlos Fernandez Lopez

Institute of Measurement and Control Systems
Karlsruhe Institute of Technology (KIT)

Christoph Stiller

Institute of Measurement and Control Systems
Karlsruhe Institute of Technology (KIT)

February 14, 2023

ABSTRACT

Self-supervised learning, which is strikingly referred to as the dark matter of intelligence, is gaining more attention in biomedical applications of deep learning. In this work, we introduce a novel self-supervision objective for the analysis of cells in biomedical microscopy images. We propose training deep learning models to pseudo-colorize masked cells. We use a physics-informed pseudo-spectral colormap that is well suited for colorizing cell topology. Our experiments reveal that approximating semantic segmentation by pseudo-colorization is beneficial for subsequent fine-tuning on cell detection. Inspired by the recent success of masked image modeling, we additionally mask out cell parts and train to reconstruct these parts to further enrich the learned representations. We compare our pre-training method with self-supervised frameworks including contrastive learning (SimCLR), masked autoencoders (MAEs), and edge-based self-supervision. We build upon our previous work and train hybrid models for cell detection, which contain both convolutional and vision transformer modules. Our pre-training method can outperform SimCLR, MAE-like masked image modeling, and edge-based self-supervision when pre-training on a diverse set of six fluorescence microscopy datasets. Code is available at: <https://github.com/roydenwa/cell-centroid-former>

Keywords Self-supervised learning, pseudo-colorization, masked image modeling, physics-informed, vision transformer, convolutional neural network

1 Introduction

The ambitious goal of deep learning research is to develop intelligent generalist models that can solve a wide variety of tasks. Supervised learning with massive amounts of labeled data does not scale to the complexity of this goal. In self-supervised learning, however, supervisory signals are generated from unlabeled data, making it more scalable. Therefore, self-supervised learning, which is strikingly referred to as the dark matter of intelligence [LeCun and Misra, 2021], is gaining more attention in many applications of deep learning. Especially in biomedical applications, where labeling data often requires support of trained experts, self-supervised learning can accelerate research progress and reduce costs [Ghesu et al., 2022]. In this work, we introduce a novel self-supervision objective for the analysis of cells in biomedical microscopy images. In contrast to recent methods for self-supervised learning on cell images (e.g., Ciga et al. [2022], Perakis et al. [2021]), we do not use contrastive learning [Hadsell et al., 2006], but propose a unique self-supervision objective tailored to cell images. We propose training deep learning models to pseudo-colorize masked cells. We use a physics-informed pseudo-spectral colormap that is well suited for colorizing cell topology. Compared to a spectral colormap, the used colormap has a higher color variance for low intensity levels. Therefore, this pseudo-spectral colormap can better highlight cell nuclei and their surroundings in areas of low intensity and low

*Corresponding author: royden.wagner@kit.edu

contrast in microscopy images. Inspired by the recent success of masked image modeling (e.g., He et al. [2022], Bao et al. [2022]), we additionally mask out cell parts to increase the complexity of the objective and further enrich the learned representations. Furthermore, we build upon our previous work [Wagner and Rohr, 2022a] and train hybrid models for cell detection, which contain both convolutional and vision transformer modules. The convolutional modules are used to capture local information, while the vision transformer modules are used to capture global information. Overall, the contributions of our work are twofold:

1. We propose a novel self-supervision objective for the analysis of biomedical cell images that combines pseudo-colorizing and masked image modeling.
2. We use a recent deep learning model for cell detection, which contains both convolutional and vision transformer modules, to evaluate the proposed self-supervision objective.

2 Related Work

Self-supervised learning on biomedical cell images. Ciga et al. [2022] and Perakis et al. [2021] use contrastive learning and build upon SimCLR [Chen et al., 2020] to train deep learning models in a self-supervised manner on cell images. In contrastive learning for visual representations, the learning objective is to maximize agreement between two different augmented views of a single sample, while using the remaining samples in a batch as negative examples. Experiments show that large batch sizes and correspondingly huge datasets and computational resources are needed to maximize performance (e.g., a batch size of 32k for SimCLR on ImageNet). Dmitrenko et al. [2022] show that a small convolutional autoencoder (only 190k parameters) trained on cell images can outperform much larger general purpose pre-trained models (e.g., ViT-B/8 [Caron et al., 2021], 85M parameters) on classifying drug effects. This demonstrates the potential of autoencoding as pre-training on cell images. However, recent work on autoencoders (e.g., He et al. [2022], Gao et al. [2022]) suggests that masking parts of the input further enriches the learned representations. Kobayashi et al. [2022] propose protein identification as self-supervision objective for pre-training on biomedical cell images. While being well tailored to cell images, this approach requires basic annotations of protein IDs. Dawoud et al. [2022] use edge detection as self-supervision objective to pre-train deep learning models for cell segmentation. Edge detection is closely related to accurate segmentation of cell borders, but is a fairly simple task which could lead to less expressive learned features.

Colorizing as self-supervision objective. Zhang et al. [2016] convert natural color images to grayscale and use the recolorization to the CIE lab color space as self-supervision objective. Vondrick et al. [2018] leverage the temporal coherency of color in natural videos to learn colorizing following frames based on a reference frame. Both approaches are promising for natural images or videos, but exploit color-related features that are not present in biomedical grayscale microscopy images.

3 Method

3.1 Pseudo-colorize Masked Cells as Self-supervision Objective

Autoencoders [Kramer, 1991] are classical deep learning models for self-supervised representation learning. During training an autoencoder learns to map its input to a latent representation and to reconstruct the input from the latent representation. The general architecture of an autoencoder contains a contracting part called encoder and an expanding part for reconstruction called decoder. Popular applications include compression, where the learned latent representation is smaller than the input, or denoising [Vincent et al., 2008], where input signals are corrupted by noise and uncorrupted signals are reconstructed. In this work, we use a new form of autoencoding by training to reconstruct pseudo-colored versions of input images. Specifically, we train deep learning models to pseudo-colorize cell images as self-supervised pre-training for cell detection. As previously shown [Dmitrenko et al., 2022], basic autoencoding of cell images can improve the performance on downstream tasks such as drug effect classification. We argue that reconstructing a pseudo-colored version is more difficult than reconstructing the original input image. Thus, it can lead to more expressive learned features and further improve the performance on downstream tasks. Figure 1 (a) shows pseudo-colored cell images and the characteristics of the used colormaps. We are using colormaps provided by the matplotlib library [Barrett et al., 2005]. The grayscale plots of the colormaps are generated by computing the perceived brightness B_P from RGB values using the HSP color system [Finley, 2006], as follows:

$$B_P = \sqrt{0.299R^2 + 0.587G^2 + 0.114B^2} \quad (1)$$

We select four colormaps from different colormap categories to cover a wide range of colormaps in the following. The rainbow colormap is a physics-informed spectral colormap based on the visible spectrum of light. The lowest intensity

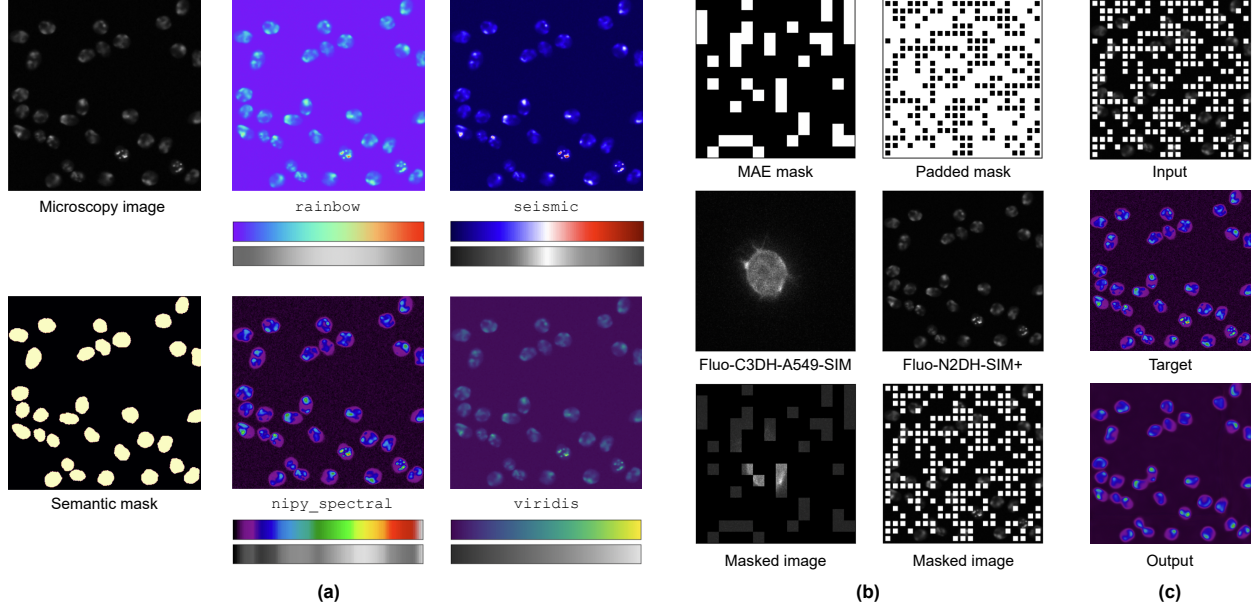


Figure 1: **(a)** Pseudo-colorization of fluorescence microscopy images and the corresponding colormaps. **(b)** Masking schemes and masked fluorescence microscopy images. MAE [He et al., 2022] masks cover 75% of images, whereas our proposed padded masks contain smaller patches and cover 33%. Image areas masked by our padded masking scheme are highlighted in white here to enhance their visibility. During pre-training, these areas are set to zero. **(c)** Proposed pre-training objective: Pseudo-colorize masked cells.

levels are mapped to violette, the highest intensity levels to red. The perceived brightness gradually decreases from medium intensity levels towards low and high intensity levels. The *seismic* colormap is a monotonically diverging colormap composed of two colors, blue and red. The perceived brightness rapidly decreases from medium intensity levels towards low and high intensity levels. The *nipy_spectral* colormap is a physics-informed pseudo-spectral color map that extends spectral colormaps by prepending black for low intensity levels and appending gray for high intensity levels. Therefore, this colormap has a higher color variance than spectral colormaps. Furthermore, the color transitions in the colormap are sharper than in spectral colormaps. This is further expressed in a less uniform perceived brightness. *viridis* is a perceptually uniform sequential colormap composed of violette, blue, green, and yellow. It contains smooth color transitions and the perceived brightness is gradually increasing from low intensity levels towards high intensity levels.

We propose to choose colormaps for pseudo-color autoencoding, where the generated color channels approximately match the semantics of the data. We hypothesise that approximating semantic segmentation by pseudo-colorization is beneficial for self-supervised pre-training on images. For data such as fluorescence microscopy images, where semantics are closely related to grayscale intensity levels, spectral or pseudo-spectral colormaps are suitable. Such colormaps map low intensities primarily to bluish colors, medium intensities to greenish colors and high intensities to reddish colors. Thus, the intensity levels are roughly divided into the three color channels in the RGB scheme and semantic segmentation is approximated. As shown in Figure 1 (a), the semantic cell mask covers primarily areas of low intensity. Therefore, the pseudo-spectral *nipy_spectral* colormap, which has a higher color variance for such intensity levels, can better highlight cells in this context than the spectral *rainbow* colormap. In detail, cell bodies are primarily colored in violette, which maps to the blue and red RGB channels, and cell nuclei are primarily colored in blue and green.

Recent work on autoencoding as pre-training on images (e.g., He et al. [2022], Bao et al. [2022], Gao et al. [2022]), suggests that masked image modeling can lead to more expressive learned features than the classical reconstruction objective. In masked image modeling, images are divided into non-overlapping patches and during pre-training these patches are randomly masked out. Thereby, the objective for an autoencoder becomes to reconstruct seen and unseen parts of an image. The idea is that during pre-training an autoencoder builds up internal representations for certain object classes and learns to leverage these to reconstruct masked image parts. Masked autoencoder (MAE) [He et al., 2022] is an autoencoder model with an encoder and decoder based on the vision transformer architecture [Dosovitskiy et al., 2021]. Therefore, images of size 224×224 pixels are divided into non-overlapping 16×16 pixel patches. For an

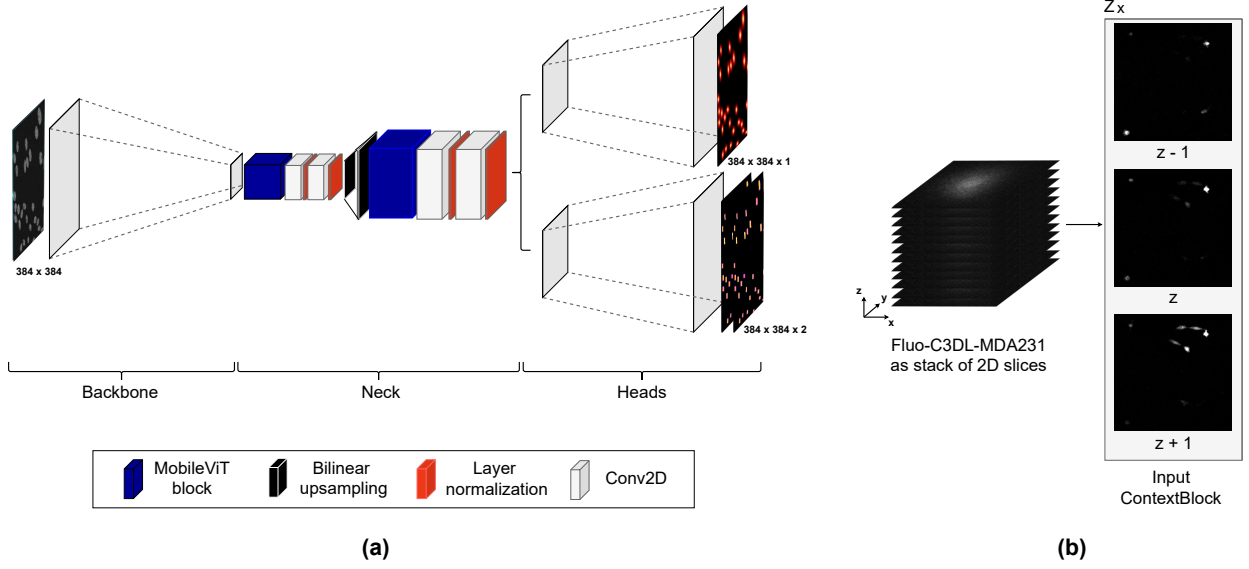


Figure 2: **(a) CellCentroidFormer model. Backbone:** Five blocks of an EfficientNetV2S [Tan and Le, 2021]. **Neck:** MobileViT blocks and convolutional layers. **Heads:** Fully convolutional upsampling blocks. **(b)** Adjacent z-slices as input for the ContextBlock.

image size of 384×384 pixels, this corresponds approximately to a patch size of 27×27 pixels. During pre-training, 75% of these patches are randomly masked out. We argue that such a masking scheme is primarily designed for data where the objective is to identify one concept per image and not to localize multiple objects within an image. As shown in Figure 1 (b), the MAE-like masking would mask out a large number of cells in a Fluo-N2DH-SIM+ microscopy image. Therefore, an autoencoder can not use partially visible cell parts as clues to reconstruct adjacent masked patches, but rather has to learn a representation for all cells combined in an image to reconstruct masked patches. In Figure 1, the MAE-like masking is therefore applied to a Fluo-C3DH-A549-SIM microscopy image, which only contains one cell. We argue that learning to leverage local or semi-local visual clues is beneficial for downstream tasks such as object detection or segmentation. Thus, we propose an alternate masking scheme for cell detection. Our padded masking scheme is composed of smaller patches (12×12 pixels for an image size of 384×384 pixels) and all patches are padded with a padding size of $1/4$ of the patch width. This surrounds all patches with a non-masked area and prevents large connected masked areas, which could mask out whole cells. The patches are masked out randomly with a probability of 50% using a discrete uniform distribution $U\{0, 1\}$ to choose the common pixel value of a patch. Considering the non-masked padding areas the overall mean masking ratio becomes 33.3%. In the following we combine the pseudo-color autoencoding with masked inputs and thus train deep learning models to pseudo-colorize masked cells.

3.2 Model Architecture

The comparison of vision transformers (ViTs) [Dosovitskiy et al., 2021] and convolutional neural networks (CNNs) [LeCun et al., 1989] in computer vision applications reveals that their receptive fields are fundamentally different [Raghu et al., 2021]. The receptive fields of ViTs capture local and global information in both earlier and later layers. The receptive fields of CNNs, on the other hand, initially capture local information and gradually grow to capture global information in later layers. Therefore, we use MobileViT blocks [Mehta and Rastegari, 2022] in the neck part of our proposed model to enhance global information compared to a fully convolutional neck part. Figure 2 (a) shows the proposed model architecture. We represent cells by their centroid, their width, and their height. Our model contains two fully convolutional heads to predict these cell properties. The first head predicts a heatmap for cell centroids, and the second head predicts the cell dimensions (width and height) at the position of the corresponding cell centroid. The heatmaps for cell centroids are generated by first creating a semantic map where cells are approximated by ellipses. Afterwards, we smooth each cell ellipse using a normalized box filter with a kernel size k that is scaled to the corresponding cell height h and width w :

$$k = (w//1.5, h//1.5), \quad (2)$$

where $//$ represents integer division. Cell height and width are encoded in rectangles sized to 50% of the corresponding cell dimensions. These rectangles contain height and width values scaled relative to the input image size of 384×384 pixels.

3.2.1 Prepended ContextBlock

The ContextBlock is a proposed extension to our CellCentroidFormer model. It serves two purposes: first, to encode spatial context from adjacent slices when analyzing 3D inputs slice-wise. Second, to provide our model with a unified input form of 3 views for 2D and 3D input data to jointly train on both types of datasets. As previously shown (e.g., Arbellet et al. [2022], Wagner and Rohr [2022b]), using triplets of adjacent slices when analyzing 3D microscopy images of cells slice-wise can improve cell detection and segmentation. Figure 2 (b) shows how we decompose a 3D microscopy images into triplets of adjacent slices. In the ContextBlock, highlevel features are first extracted from adjacent slices S using convolutional layers. These features are then merged with the current slice using a multiply-accumulate operation to generate a context tensor $T_{context}$ with three channels.

$$T_{context}(z) = \begin{bmatrix} \sigma(\text{Conv1x1}(\text{Conv3x3}(S(z-1))) \cdot S(z) + S(z)) \\ S(z) \\ \sigma(\text{Conv1x1}(\text{Conv3x3}(S(z+1))) \cdot S(z) + S(z)) \end{bmatrix}, \quad (3)$$

where Conv3x3 and Conv1x1 represent 2D convolutional layers with kernel sizes of 3×3 and 1×1 and σ represents a sigmoid activation function. A Conv3x3 layer with 10 filters is used to detect high-level features, afterwards these features are fused along the depth axis using a Conv1x1 layer with one filter. We merge context from the previous slice $S(z-1)$ in the first channel, the second channel contains the current slice $S(z)$, and context from the next slice $S(z+1)$ is merged in the third channel. In this way, context from adjacent slices can be highlighted, but the focus remains on the current slice. In general, prepending the ContextBlock is a learned 2.5D approach for 3D data. For 2D data, additional features are extracted and 3 unique views of input images are generated.

3.2.2 Decoding Predictions

When decoding predictions, we first generate a binary map E_{blob} that contains elliptical blobs by applying a threshold on the centroid heatmap $H_{centroid}$, as follows:

$$E_{blob}(x, y) = H_{centroid}(x, y) > 0.75 \quad (4)$$

Afterwards, we compute the image moments M per blob and derive the corresponding centroid position C using:

$$C\{x, y\} = \left\{ \frac{M_{10}}{M_{00}}, \frac{M_{01}}{M_{00}} \right\} \quad (5)$$

These centroid positions are then used to lookup the corresponding cell dimensions in the predicted cell height and cell width maps. In this work, we use the classic bounding box format of top left corner plus height and width as output.

4 Results

4.1 Datasets

We use publicly available datasets from the Cell Tracking Challenge [Ulman et al., 2017] to evaluate our proposed method. In the first set of experiments, we are using the Fluo-N2DH-SIM+ dataset [Svoboda and Ulman, 2016], which contains fluorescence microscopy images of simulated nuclei of HL60 cells. Figure 1 shows an example image of this dataset. In the second set of experiments, we combine the Fluo-N2DH-SIM+ with the Fluo-C3DH-A549-SIM [Sorokin et al., 2018], the Fluo-C2DL-Huh7 [Ruggieri et al., 2012], the Fluo-C3DL-MDA231, the Fluo-N2DH-GOWT1 [Bártová et al., 2011], and the Fluo-C2DL-MSD datasets for pre-training. The Fluo-C3DH-A549-SIM contains 3D fluorescence microscopy images of simulated GFP-actin-stained A549 lung cancer cells. The Fluo-C2DL-Huh7 dataset contains 2D fluorescence microscopy images of human hepatocarcinoma-derived cells expressing the fusion protein YFP-TIA-1. The Fluo-C3DL-MDA231 dataset contains 3D fluorescence microscopy images of human breast carcinoma cells infected with a pMSCV vector including the GFP sequence, which are embedded in a collagen matrix. The Fluo-N2DH-GOWT1 dataset contains 2D fluorescence microscopy images of GFP-GOWT1 mouse stem cells. The Fluo-C2DL-MSD dataset contains 2D fluorescence microscopy images of rat mesenchymal stem cells on a flat polyacrylamide substrate. Table 2 contains example images for all used datasets (2D slices for 3D datasets), in the order in which they are listed here. As pre-processing, we apply a median filter with a kernel size of 3 and perform min-max scaling. During training, we use the Fluo-N2DH-SIM+ and Fluo-C3DH-A549-SIM datasets that provide panoptic segmentation masks as ground truth, which we convert to bounding box annotations for cells.

4.2 Comparing Autoencoding Schemes Including Pseudo-colorization and Masking as Pre-training on Cell Images

In this set of experiments, we are comparing different autoencoding schemes as pre-training for cell detection. We perform two types of training procedures, fine-tuning and head evaluation. For fine-tuning, we pre-train the models using different autoencoding schemes and afterwards allow all model parameters to adapt to the downstream task during training. For head evaluation, we pre-train the models using different autoencoding schemes and afterwards freeze the weights in the backbone and neck part of our model during training. Therefore, only the heads are adapting to the downstream task, which corresponds to 17% of the total model parameters.

Table 1: **Comparing autoencoding schemes including pseudo-colorization and masking as pre-training on cell images.** As baseline, the first row shows a model trained from scratch with random weight initialization. Masking refers to our proposed padded masking scheme. Best scores per training procedure are bold, second best scores are underlined.

Pre-training			Training						
Colormap	Masking	SSIM ^{heads} _{test}	F _{DS}	AP _{test}	AP ⁵⁰ _{test}	AP ^{small} _{test}	AP ^{medium} _{test}	mIoU ^{heatmap} _{train}	T _{rel}
-	-	-	100%	31.37 (1.27)	71.93 (0.90)	27.43 (1.08)	44.37 (2.06)	82.78 (0.82)	1.0
<i>Fine-tuning:</i>									
-	-	0.9212 (0.0009)	100%	38.93 (2.60)	78.87 (2.20)	34.17 (2.40)	54.33 (3.25)	90.02 (2.04)	<u>1.9</u>
rainbow	-	0.8392 (0.0003)	100%	40.60 (1.97)	79.77 (1.00)	35.53 (1.81)	56.53 (2.65)	89.79 (1.27)	2.3
viridis	-	0.8790 (0.0087)	100%	40.70 (1.22)	80.03 (0.85)	35.97 (1.10)	56.07 (1.37)	<u>91.21</u> (0.11)	2.3
seismic	-	0.9020 (0.0035)	100%	40.33 (0.49)	79.80 (0.35)	35.73 (0.40)	55.13 (1.46)	90.41 (0.68)	2.3
nipy_spectral	-	0.6302 (0.0004)	100%	43.10 (1.51)	81.63 (0.90)	38.07 (1.02)	58.93 (2.93)	90.95 (0.50)	2.3
nipy_spectral	✓	0.6861 (0.0004)	100%	43.43 (1.90)	81.90 (1.61)	38.40 (2.15)	59.27 (1.30)	91.30 (0.55)	2.3
<i>Head evaluation:</i>									
-	-	0.9212 (0.0009)	100%	22.30 (2.69)	58.50 (4.77)	19.30 (2.60)	32.67 (2.57)	69.74 (0.86)	<u>1.6</u>
nipy_spectral	-	0.6302 (0.0004)	100%	<u>30.87</u> (4.74)	<u>69.40</u> (4.42)	<u>27.30</u> (3.81)	<u>43.00</u> (6.81)	<u>73.41</u> (0.69)	2.1
nipy_spectral	✓	0.6861 (0.0004)	100%	32.57 (1.88)	70.17 (2.77)	28.30 (1.66)	47.17 (2.33)	74.06 (0.34)	2.1
<i>Head evaluation with smaller training dataset:</i>									
-	-	0.9212 (0.0009)	20%	9.45 (2.25)	30.02 (5.91)	7.00 (1.76)	18.65 (3.39)	66.69 (0.83)	<u>1.1</u>
nipy_spectral	-	0.6302 (0.0004)	20%	16.80 (2.77)	49.07 (5.00)	14.57 (2.36)	<u>24.97</u> (4.26)	72.29 (0.62)	1.5
nipy_spectral	✓	0.6861 (0.0004)	20%	<u>15.88</u> (3.47)	<u>44.65</u> (7.92)	<u>13.28</u> (3.08)	25.78 (5.02)	<u>70.77</u> (1.17)	1.5

Dataset. As dataset, we are using the training split of the Fluo-N2DH-SIM+ dataset. We perform geometric data augmentations such as elastic, perspective, shift, scale, and rotation transformations to increase the dataset size to 2150 samples. 80% of the resulting dataset are used for training and 20% for testing. The used dataset is rather small and we are comparing similar autoencoding schemes in this set of experiments. Therefore, we perform data augmentations beforehand instead of randomly and on-the-fly during training to train all models with the exact same samples and allow a fair comparison.

Evaluation metrics. As evaluation metrics, we use the structural similarity score (SSIM) [Wang et al., 2004], the mean intersection-over-union metric (mIoU), and bounding box average precision metrics (AP). The structural similarity score measures the similarity of two matrices or grayscale images and is used to measure the reconstruction quality during pre-training. For pseudo-colored images we compute the SSIM score per color channel and average them. We do not use weight-sharing, but train both heads separately during pre-training. Therefore, we report the mean SSIM score of both model heads. The metric is defined as follows:

$$\text{SSIM}(x_1, x_2) = \frac{(2\mu_{x_1}\mu_{x_2} + (0.01L)^2)(2\sigma_{x_1x_2} + (0.03L)^2)}{(\mu_{x_1}^2 + \mu_{x_2}^2 + (0.01L)^2)(\sigma_{x_1}^2 + \sigma_{x_2}^2 + (0.03L)^2)} \quad (6)$$

For two inputs, the mean μ , the variance σ , and the dynamic range L are computed. The mIoU metric is used to evaluate the centroid heatmap predictions. Matching our decoding procedure in Equation 4, we apply a threshold to the predicted and ground truth heatmap before computing the mIoU score. The metric is defined as:

$$\text{mIoU} = \frac{1}{C} \sum_C \frac{TP_C}{TP_C + FP_C + FN_C} \quad (7)$$

For the two class labels C , background and cell centroid blobs, the true positive TP , false positive FP , and false negative FN pixels are computed. The bounding box AP metrics are computed using the pycocotools software library, we refer to the COCO dataset [Lin et al., 2014] for more details.

Experimental setup. During pre-training, Adam [Kingma and Ba, 2015] with its standard configuration is used as optimizer, the initial learning rate is set to 1^{-4} , and reduced on plateaus by a factor of 10 to a minimum learning rate of 1^{-6} . As pre-training loss, we are computing the pixel-wise mean squared error (MSE) between the reconstructed and the original microscopy images. All autoencoding schemes including pseudo-colorization are pre-trained for 75 epochs, whereas the basic autoencoding without pseudo-colorization is pre-trained for 50 epochs since it converges faster. Therefore, the basic autoencoding scheme has a lower relative total training time T_{rel} than the remaining autoencoding schemes. During training, the same optimizer configuration and learning rate scheduling are used. As training loss, three Huber loss functions [Huber, 1964] are used, one loss function per output (heatmap, height, and width). The total loss is computed by a weighted sum of the three loss values:

$$\mathcal{L}_{Huber}(y, \hat{y}) = \begin{cases} \frac{1}{2}(y - \hat{y})^2 & \text{if } y - \hat{y} \leq 1.0, \\ (y - \hat{y}) - \frac{1}{2} & \text{else} \end{cases} \quad (8)$$

$$\mathcal{L}_{total} = \mathcal{L}_{heatmap} + \frac{1}{2} \cdot \mathcal{L}_{height} + \frac{1}{2} \cdot \mathcal{L}_{width} \quad (9)$$

All models are trained for 50 epochs to detect cells. All training runs are completed three times, Table 1 shows the mean and standard deviation for all considered metrics.

Results. Basic autoencoding without pseudo-colorization yields the highest SSIM scores during pre-training, autoencoding using the `viridis` and `seismic` colormaps yields the second highest SSIM scores. This shows that these pre-training objectives are simpler than the remaining ones and therefore easier to learn. More difficult to learn seems autoencoding using the `spectral rainbow` colormap and most difficult are the two variations with and without masking using the `pseudo-spectral nipy_spectral` colormap. For all autoencoding schemes, the standard deviation from the SSIM score are low, showing that both model heads learn the objectives similarly well. In the fine-tuning training procedure, all autoencoding schemes achieve at least 10% higher values in all metrics than the baseline model trained from scratch. This demonstrates that autoencoding is generally an effective form of pre-training for this type of data. All cells in the Fluo-N3DH-SIM+ dataset fall into the small and medium large object categories with respect to COCO AP metrics. In general, medium sized cells are better detected, which is shown by higher AP scores. The basic autoencoding achieves on average about 2% lower AP scores than the very similar performing autoencoding schemes with the `rainbow`, `viridis`, and `seismic` colormaps. The two autoencoding schemes with the `nipy_spectral` colormap achieve AP scores that are about another 2.5% higher. When comparing these two autoencoding schemes, the autoencoding scheme that uses the proposed padded masking in addition to the `nipy_spectral` colormap achieves AP values that are consistently about 0.3% higher and thus performs best. The mIoU scores, which are achieved during training, are close to each other in this training procedure and within a range of 1.5%. In the following head evaluation procedure, the two previously best performing autoencoding schemes are compared with the basic autoencoding scheme. According to the significantly lower number of parameters, which can adapt to the downstream task, the performance drops significantly. On average, 10 to 20% lower AP scores are achieved. The performance differences between the three autoencoding schemes are comparable to those from the previous procedure. Therefore, the autoencoding scheme using the combination of `nipy_spectral` colormap and padded masking again performs best. This autoencoding scheme is also the only one that outperforms the differently trained baseline model with this training procedure. We increase the difficulty further by reducing the fraction of the training dataset F_{DS} used to 20%. With this setup, the achieved AP scores are approximately halved. The two autoencoding schemes with the `nipy_spectral` colormap outperform the basic autoencoding again, whereas the autoencoding scheme with the `nipy_spectral` colormap but without masking performs best in this setup. We hypothesize that the task switch from pure pseudo-colorization to cell detection is easier and therefore can be learned better with fewer training samples. The additional masking arguably enhances the learned representations, leading to better performance in the previous experimental setups. However, the associated reconstruction of masked image parts differs more than the pure pseudo-colorization from cell detection using centroid representations.

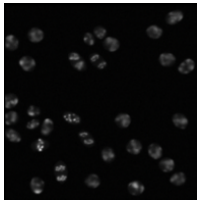

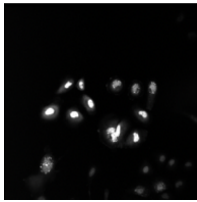
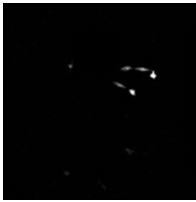
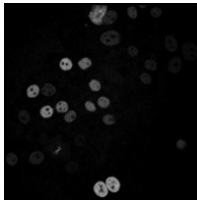
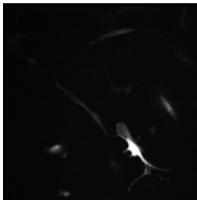
4.3 Comparing Self-supervised Pre-training Methods on Cell Images

In this set of experiments, we are comparing our proposed pre-training objective, pseudo-colorizing masked cells (PMC), with recent methods for self-supervised pre-training on cell images. Following Ciga et al. [2022], we pre-train our model using the contrastive learning framework SimCLR. In addition, we compare our method with edge-based self-supervision (EdgeSSV) [Dawoud et al., 2022] and pure masked image modeling with the masking scheme of masked autoencoders (MAE) [He et al., 2022]. The performance comparison is performed with backbone evaluation as training procedure. For this, the weights in the backbone are frozen after the pre-training, so that only the neck part and the two heads of our model adapt to the downstream task of cell detection.

Experimental setup. As described in Section 4.1, we pre-train with a diverse set of 6 fluorescence microscopy datasets. Subsequent training to evaluate performance is performed on the Fluo-C3DH-A549-SIM and the Fluo-N2DH-SIM+

datasets. The pre-training of all methods is performed for 75 epochs, the subsequent training for 50 epochs. During pre-training and training, we use the same optimizer setup and learning rate schedule as in Section 4.2 for all methods. During pre-training, we randomly perform geometric data augmentations on-the-fly such as flip, rotation, and crop transformations. An exception is the pre-training of SimCLR, where color affine transformations are performed in addition to geometric augmentations, as specified in the framework [Chen et al., 2020]. For color affine transformations, the prepended ContextBlock in our model and the corresponding input tensors with 3 channels additionally serve as adapters to apply such transformations to grayscale images. For SimCLR, we restrict the extent of the geometric augmentations, since the datasets used were created from time-lapse microscopy videos. In these videos, cells move only moderately between frames, so that successive frames are very similar. For contrastive learning, this means that strong geometric augmentations would lead to two differently augmented views of the same frame being more different from each other than from surrounding frames. However, since all frames except the two views of the same frame are used as negative samples in contrastive learning, we limit the extent of geometric transformations to only slight rotations ($\pm 10^\circ$) and cropping to a minimum of 90% of the original size. For SimCLR-pre-training, we replace the two model heads by one projection head with three fully connected layers, which have 256, 128, and 64 nodes. For the remaining methods, the architecture of our CellCentroidFormer model is not changed, only the top-layer is switched according to the output format between pre-training and training. Training runs are performed three times, we report mean and standard deviation in Table 2.

Table 2: **Comparing self-supervised pre-training methods on cell images.** Best scores are bold, second best scores are underlined. A549-SIM and N2DH-SIM+ refer to the Fluo-C3DH-A549-SIM and Fluo-N2DH-SIM+ datasets.

Pre-training datasets							
							
N2DH-SIM+		A549-SIM		Huh7		MDA231	
							
GOWT1		MSC					
Pre-training method	Det. dataset	AP_{test}	AP_{test}^{50}	AP_{test}^{small}	AP_{test}^{medium}	AP_{test}^{large}	$mIoU_{train}^{heatmap}$
SimCLR	A549-SIM	24.40 (2.69)	75.50 (0.99)	- (-)	24.20 (2.12)	27.10 (3.25)	71.33 (1.21)
MAE-like	A549-SIM	<u>57.43</u> (2.23)	86.13 (1.75)	- (-)	<u>49.83</u> (2.71)	71.30 (2.75)	94.30 (1.08)
EdgeSSV	A549-SIM	55.70 (3.11)	<u>87.35</u> (2.90)	- (-)	47.10 (3.25)	<u>70.40</u> (2.97)	93.04 (0.15)
PMC (Ours)	A549-SIM	57.70 (3.54)	87.90 (1.41)	- (-)	51.80 (2.97)	70.00 (3.11)	<u>93.08</u> (0.80)
SimCLR	N2DH-SIM+	24.10 (0.99)	60.55 (1.06)	20.10 (0.99)	37.45 (0.92)	- (-)	68.10 (1.72)
MAE-like	N2DH-SIM+	27.25 (1.34)	66.55 (1.63)	23.40 (1.13)	39.85 (1.77)	- (-)	84.78 (1.44)
EdgeSSV	N2DH-SIM+	<u>31.30</u> (0.71)	<u>72.50</u> (1.41)	<u>26.95</u> (0.64)	<u>45.20</u> (0.57)	- (-)	86.23 (1.29)
PMC (Ours)	N2DH-SIM+	33.75 (0.64)	73.10 (0.57)	28.90 (0.85)	49.25 (0.64)	- (-)	<u>85.15</u> (1.06)

Results. As expected, all methods perform better on the Fluo-C3DH-A549-SIM dataset than on the Fluo-N2DH-SIM+ dataset, which contains 3D data but only one cell is visible per frame. Furthermore, this dataset does not contain small cells, accordingly we can not compare AP_{test}^{small} scores. The cells in this 3D dataset have an ellipsoidal shape, therefore their size in 2D slices decreases from the center of the volume to the border. Accordingly, the detection in 2D slices from the center of the volume is evaluated with the AP_{test}^{large} metric, and towards the border with the AP_{test}^{medium} metric. In the inner 2D slices, cells are detected more accurately by all methods. On the Fluo-N2DH-SIM+ dataset, medium sized cells are detected more accurately than small cells by all methods. On both datasets, SimCLR performs worst overall, which can be explained by the fact that the similarity between individual frames in time-lapse videos makes training for SimCLR more challenging. MAE-like masking performs significantly worse on the Fluo-N2DH-SIM+ dataset than on the Fluo-C3DH-A549-SIM dataset. This supports our hypothesis that this masking scheme is better suited for data with one concept (one cell) per image. On the Fluo-C3DH-A549-SIM dataset, MAE-like masking performs second best and yields AP_{test} scores within 1% of our proposed method. The EdgeSSV method achieves high AP scores on both datasets. Overall, our proposed method achieves the highest AP scores on both datasets. However, considering that on the Fluo-C3DH-A549-SIM dataset the three best methods yield AP_{test} scores within a range of 2% and the higher standard deviation values, the performance difference is less significant for this dataset. Interestingly, our method does not achieve the highest $mIoU_{train}^{heatmap}$ scores in either dataset, which is measured on the training data. This suggests that our method generalizes better and other methods tend to overfit somewhat more on the training data.

5 Discussion

Our experiments reveal that pseudo-colorization is an effective extension to autoencoding for pre-training on cell images. Pseudo-color autoencoding with pseudo-spectral colormaps, which approximate the semantics of cell images, yields the best results on fluorescence microscopy images. As recently shown for natural images [Assran et al., 2022], the combination of standalone self-supervision objectives with masked image modeling can also further improve performance on biomedical cell images. The proposed unique combination of pseudo-color autoencoding and masked image modeling for cell images can outperform several autoencoding schemes, contrastive learning, and edge-based self-supervision. Our proposed masking scheme consists of smaller patches and covers a much smaller area of images than the typical masking scheme of masked autoencoders. This prevents object instances from being completely masked. We found this to be beneficial for subsequent training on object detection in our experiments. Our CellCentroidFormer model has no special mechanism to suppress the artificial edges added by masking. Nevertheless, as shown in Figure 1 (c), no edge artifacts are visible in the reconstructions. We hypothesize that the self-attention layers in the neck part of our model help to suppress these edge artifacts, since self-attention can be understood as a form of generalized spatial smoothing [Park and Kim, 2021]. However, it is plausible that our method can be further improved by using masked convolutions [Gao et al., 2022] instead of regular convolutions to suppress artificial edges. Moreover, we do not achieve the computational efficiency of masked autoencoders where only unmasked patches are processed in the encoder. These are possible future directions of our work. To this end, we show that our proposed pre-training method can achieve good performance on small cell image datasets using an autoencoder-like model without special architectural modifications.

References

- Yann LeCun and Ishan Misra. Self-supervised learning: The dark matter of intelligence. <https://ai.facebook.com/blog/self-supervised-learning-the-dark-matter-of-intelligence>, 2021. Accessed: 2022-08-01.
- Florin C Ghesu, Bogdan Georgescu, Awais Mansoor, Youngjin Yoo, Dominik Neumann, Pragneshkumar Patel, RS Vishwanath, James M Balter, Yue Cao, Sasa Grbic, et al. Self-supervised learning from 100 million medical images. *arXiv preprint arXiv:2201.01283*, 2022.
- Ozan Ciga, Tony Xu, and Anne Louise Martel. Self supervised contrastive learning for digital histopathology. *Machine Learning with Applications*, 7:100198, 2022.
- Alexis Perakis, Ali Gorji, Samriddhi Jain, Krishna Chaitanya, Simone Rizza, and Ender Konukoglu. Contrastive learning of single-cell phenotypic representations for treatment classification. In *Machine Learning in Medical Imaging*, pages 565–575, 2021.
- Raia Hadsell, Sumit Chopra, and Yann LeCun. Dimensionality reduction by learning an invariant mapping. In *Conference on Computer Vision and Pattern Recognition*, volume 2, pages 1735–1742. IEEE, 2006.
- Kaiming He, Xinlei Chen, Saining Xie, Yanghao Li, Piotr Dollár, and Ross Girshick. Masked autoencoders are scalable vision learners. In *Conference on Computer Vision and Pattern Recognition*, pages 16000–16009. IEEE/CVF, 2022.
- Hangbo Bao, Li Dong, Songhao Piao, and Furu Wei. Beit: Bert pre-training of image transformers. In *International Conference on Learning Representations*, 2022.
- Royden Wagner and Karl Rohr. CellCentroidFormer: Combining Self-attention and Convolution for Cell Detection. In *Medical Image Understanding and Analysis*, pages 212–222. Springer, 2022a.
- Ting Chen, Simon Kornblith, Mohammad Norouzi, and Geoffrey Hinton. A simple framework for contrastive learning of visual representations. In *International Conference on Machine Learning*, pages 1597–1607. PMLR, 2020.
- Andrei Dmitrenko, Mauro Miguel Masiero, and Nicola Zamboni. Self-supervised learning for analysis of temporal and morphological drug effects in cancer cell imaging data. In *Medical Imaging with Deep Learning*, 2022.
- Mathilde Caron, Hugo Touvron, Ishan Misra, Hervé Jégou, Julien Mairal, Piotr Bojanowski, and Armand Joulin. Emerging properties in self-supervised vision transformers. In *International Conference on Computer Vision*, pages 9650–9660, 2021.
- Peng Gao, Teli Ma, Hongsheng Li, Jifeng Dai, and Yu Qiao. Convmae: Masked convolution meets masked autoencoders. In *Conference on Neural Information Processing*, 2022.
- Hirofumi Kobayashi, Keith C Cheveralls, Manuel D Leonetti, and Loic A Royer. Self-supervised deep learning encodes high-resolution features of protein subcellular localization. *Nature methods*, pages 1–9, 2022.
- Youssef Dawoud, Katharina Ernst, Gustavo Carneiro, and Vasileios Belagiannis. Edge-based self-supervision for semi-supervised few-shot microscopy image cell segmentation. *Medical Optical Imaging and Virtual Microscopy Image Analysis*, 2022.

- Richard Zhang, Phillip Isola, and Alexei A Efros. Colorful image colorization. In *European Conference on Computer Vision*, pages 649–666. Springer, 2016.
- Carl Vondrick, Abhinav Shrivastava, Alireza Fathi, Sergio Guadarrama, and Kevin Murphy. Tracking emerges by colorizing videos. In *European Conference on Computer Vision*, pages 391–408. Springer, 2018.
- Mark A Kramer. Nonlinear principal component analysis using autoassociative neural networks. *AIChE journal*, 37(2): 233–243, 1991.
- Pascal Vincent, Hugo Larochelle, Yoshua Bengio, and Pierre-Antoine Manzagol. Extracting and composing robust features with denoising autoencoders. In *Proceedings of the 25th international conference on Machine learning*, pages 1096–1103, 2008.
- Paul Barrett, John Hunter, J Todd Miller, J-C Hsu, and Perry Greenfield. matplotlib—a portable python plotting package. In *Astronomical data analysis software and systems XIV*, volume 347, page 91, 2005.
- Darel Rex Finley. Hsp color model — alternative to hsv (hsb) and hsl. <https://alienryderflex.com/hsp.html>, 2006. Accessed: 2022-09-10.
- Alexey Dosovitskiy, Lucas Beyer, Alexander Kolesnikov, Dirk Weissenborn, Xiaohua Zhai, Thomas Unterthiner, Mostafa Dehghani, Matthias Minderer, Georg Heigold, Sylvain Gelly, et al. An image is worth 16x16 words: Transformers for image recognition at scale. In *International Conference on Learning Representations*, 2021.
- Yann LeCun, Bernhard Boser, John S Denker, Donnie Henderson, Richard E Howard, Wayne Hubbard, and Lawrence D Jackel. Backpropagation applied to handwritten zip code recognition. *Neural computation*, 1(4):541–551, 1989.
- Maithra Raghu, Thomas Unterthiner, Simon Kornblith, Chiyuan Zhang, and Alexey Dosovitskiy. Do vision transformers see like convolutional neural networks? In *Advances in Neural Information Processing Systems*, volume 34, pages 12116–12128, 2021.
- Sachin Mehta and Mohammad Rastegari. Mobilevit: Light-weight, general-purpose, and mobile-friendly vision transformer. In *International Conference on Learning Representations*, 2022.
- Mingxing Tan and Quoc Le. Efficientnetv2: Smaller models and faster training. In *International Conference on Machine Learning*, pages 10096–10106. PMLR, 2021.
- Assaf Arbelle, Shaked Cohen, and Tammy Riklin Raviv. Dual-task convlstm-unet for instance segmentation of weakly annotated microscopy videos. *IEEE Transactions on Medical Imaging*, 2022.
- Royden Wagner and Karl Rohr. Efficientcellseg: Efficient volumetric cell segmentation using context aware pseudocoloring. In *Medical Imaging with Deep Learning*, 2022b.
- Vladimír Ulman, Martin Maška, Klas EG Magnusson, Olaf Ronneberger, Carsten Haubold, Nathalie Harder, Pavel Matula, Petr Matula, David Svoboda, Miroslav Radojevic, et al. An objective comparison of cell-tracking algorithms. *Nature methods*, 14(12):1141–1152, 2017.
- David Svoboda and Vladimír Ulman. Mitogen: a framework for generating 3d synthetic time-lapse sequences of cell populations in fluorescence microscopy. *IEEE transactions on medical imaging*, 36(1):310–321, 2016.
- Dmitry V Sorokin, Igor Peterlík, Vladimír Ulman, David Svoboda, Tereza Nečasová, Katsiarina Morgaenko, Livia Eiselleová, Lenka Tesařová, and Martin Maška. Filogen: a model-based generator of synthetic 3-d time-lapse sequences of single motile cells with growing and branching filopodia. *IEEE Transactions on Medical Imaging*, 37(12):2630–2641, 2018.
- Alessia Ruggieri, Eva Dazert, Philippe Metz, Sarah Hofmann, Jan-Philip Bergeest, Johanna Mazur, Peter Bankhead, Marie-Sophie Hiet, Stephanie Kallis, Gualtiero Alvisi, et al. Dynamic oscillation of translation and stress granule formation mark the cellular response to virus infection. *Cell host & microbe*, 12(1):71–85, 2012.
- Eva Bártová, Gabriela Šustáčková, Lenka Stixová, Stanislav Kozubek, Soňa Legartová, and Veronika Foltánková. Recruitment of oct4 protein to uv-damaged chromatin in embryonic stem cells. *PLoS One*, 6(12):e27281, 2011.
- Zhou Wang, Alan C Bovik, Hamid R Sheikh, and Eero P Simoncelli. Image quality assessment: from error visibility to structural similarity. *IEEE transactions on image processing*, 13(4):600–612, 2004.
- Tsung-Yi Lin, Michael Maire, Serge Belongie, James Hays, Pietro Perona, Deva Ramanan, Piotr Dollár, and C Lawrence Zitnick. Microsoft coco: Common objects in context. In *European conference on computer vision*, pages 740–755. Springer, 2014.
- Diederik P Kingma and Jimmy Ba. Adam: A method for stochastic optimization. In *International Conference for Learning Representations*, 2015.
- Peter J Huber. Robust Estimation of a Location Parameter. *Annals of Statistics*, 53:73–101, 1964.

Mahmoud Assran, Mathilde Caron, Ishan Misra, Piotr Bojanowski, Florian Bordes, Pascal Vincent, Armand Joulin, Mike Rabbat, and Nicolas Ballas. Masked siamese networks for label-efficient learning. In *European Conference on Computer Vision*, pages 456–473. Springer, 2022.

Namuk Park and Songkuk Kim. How do vision transformers work? In *International Conference on Learning Representations*, 2021.